tvst

https://doi.org/10.1167/tvst.7.4.4

Article

# Parafoveal Nonperfusion Analysis in Diabetic Retinopathy Using Optical Coherence Tomography Angiography

Brian D. Krawitz[1,2], Erika Phillips[3], Richard D. Bavier[2], Shelley Mo[1,2], Joseph Carroll[3,4,5], Richard B. Rosen[1,2], and Toco Y. P. Chui[1,2]

[1] Icahn School of Medicine at Mount Sinai, New York City, NY, USA
[2] Ophthalmology, New York Eye and Ear Infirmary of Mount Sinai, New York City, NY, USA
[3] Ophthalmology and Visual Sciences, Medical College of Wisconsin, Milwaukee, WI, USA
[4] Biophysics, Medical College of Wisconsin, Milwaukee, WI, USA
[5] Cell Biology, Neurobiology and Anatomy, Medical College of Wisconsin, Milwaukee, WI, USA

**Correspondence:** Toco Y. P. Chui, 310 E 14th St, 5th Floor, South Building, New York City, NY 10003, USA. e-mail: ychui@nyee.edu

**Received:** 1 February 2018
**Accepted:** 22 May 2018
**Published:** 12 July 2018

**Keywords:** diabetic retinopathy; nonperfusion; intercapillary areas; optical coherence tomography angiography

**Citation:** Krawitz BD, Phillips E, Bavier RD, Mo S, Carroll J, Rosen RB, Chui TYP. Parafoveal nonperfusion analysis in diabetic retinopathy using optical coherence tomography angiography. Trans Vis Sci Tech. 2018;7(4):4, https://doi.org/10.1167/tvst.7.4.4



**Purpose:** To describe a new technique for mapping parafoveal intercapillary areas (PICAs) using optical coherence tomography angiography (OCTA), and demonstrate its utility for quantifying parafoveal nonperfusion in diabetic retinopathy (DR).

**Methods:** Nineteen controls, 15 diabetics with no retinopathy (noDR), 15 with nonproliferative diabetic retinopathy (NPDR), and 15 with proliferative diabetic retinopathy (PDR) were imaged with 10 macular OCTA scans. PICAs were automatically delineated on the averaged superficial OCTA images. Following creation of an eccentricity-specific reference database from the controls, all PICAs greater than 2 SD above the reference means for PICA area and minor axis length were identified as nonperfused areas. Regions of interest (ROI) at 300 μm and 1000 μm from the foveal avascular zone (FAZ) margin were analyzed. Percent nonperfused area was defined as summed nonperfused areas divided by ROI area. Values were compared using Kruskal-Wallis and post-hoc Mann-Whitney *U* tests.

**Results:** Median values for total percent nonperfused area at the 300-μm ROI were 2.09, 2.44, 18.08, and 27.55 in the control, noDR, NPDR, and PDR groups, respectively. Median values at the 1000-μm ROI were 3.10, 3.31, 13.42, and 23.00. While there were no significant differences between the control and noDR groups, significant differences were observed between all other groups at both ROIs.

**Conclusions:** Percent nonperfused area can quantify parafoveal nonperfusion in DR and can be calculated through automatic delineation of PICAs in an eccentricity-specific manner using a standard deviation mapping approach.

**Translational Relevance:** Percent nonperfused area shows promise as a metric to measure disease severity in diabetic retinopathy.

## Introduction

Macular nonperfusion is a critical feature of diabetic retinopathy (DR) that can lead to significant visual impairment.[1–11] Microvascular dysfunction in DR causes hypoperfusion and retinal hypoxia,[12–18] and at the macula it threatens the tissue responsible for central visual acuity. While macular nonperfusion has been shown to be a risk factor for progression to more advanced disease,[19] diabetic patients with poor macular perfusion are often asymptomatic until the later stages when vision loss can be acute and severe.[1] Additionally, the presence of significant macular nonperfusion can limit the benefits of treatment.[19–22] Therefore, identification and quantification of these microvascular changes is essential to assess disease severity and guide optimal management to prevent vision loss.

Intravenous fluorescein angiography (IVFA) is a frequently used imaging modality to evaluate nonperfusion in DR.[23–28] Many efforts to quantify macular nonperfusion using IVFA have focused on

the foveal avascular zone (FAZ), demonstrating enlargement and irregularity of this region in DR that suggest capillary dropout.[23–26,29,30] IVFA has also been used to measure parafoveal intercapillary areas (PICAs), showing PICA enlargement in DR.[10,24,29–32] However, the majority of these methods have been manual and labor-intensive, and they only provide a global index of nonperfusion. Additionally, IVFA is limited in its image quality and resolution of the fine foveal vasculature,[30,33–35] can obscure capillary details secondary to dye leakage,[36,37] and is an invasive procedure that is associated with a variety of side effects.[38–40]

Newer efforts to visualize the macular blood vessels and quantify nonperfusion have been successfully demonstrated using optical coherence tomography angiography (OCTA),[36,41–50] a modality that utilizes motion contrast to generate perfusion maps, obviating the need for extrinsic dye injection. Recently, automatic computation of vascular perfusion density at the macula using OCTA has shown promise as a way to quickly evaluate perfusion status in DR.[43,49,50] While this metric can measure nonperfusion globally, identification of focal defects remains difficult. Individual variations in major blood vessel patterns and FAZ size that affect perfusion density values at changing retinal eccentricities have made the creation of a reference database for focal detection of perfusion abnormalities elusive.

Few studies have utilized OCTA to measure PICAs as a method to evaluate macular nonperfusion,[46–48] with limited quantification techniques that focus on global nonperfusion analysis. In this study, we used OCTA to measure PICAs and quantify areas of nonperfusion in both healthy controls and diabetics, employing a unique method that was both automatic and retinal eccentricity–specific based on their creation of a reference database. We demonstrated how this non-invasive technique can not only detect global nonperfusion, but can also localize focal defects.

# Methods

## Subjects

This cross-sectional study was conducted in accordance with the tenets of the Declaration of Helsinki and was approved by the Institutional Review Boards at both the New York Eye and Ear Infirmary of Mount Sinai and the Medical College of Wisconsin. For this study, we recruited 19 control subjects with no history of intraocular pathology or major systemic vascular disease. We also recruited 45 diabetic subjects with varying levels of retinopathy: 15 with no clinically observable diabetic retinopathy (noDR), 15 with nonproliferative diabetic retinopathy (NPDR), and 15 with proliferative diabetic retinopathy (PDR). Patient diagnoses and previous treatment status were determined by thorough chart review. Inclusion criteria were as follows: normal anterior segment, clear natural lens, clear media, and best corrected visual acuity better than 20/80. Exclusion criteria included nuclear, cortical, or posterior subcapsular cataracts $\geq$ grade 3 according to the Lens Opacity Classification System III;[51] prior refractive surgery; active macular edema; concomitant retinal pathology such as venous or arterial occlusions; and systemic vascular conditions such as sickle cell disease, HIV, or uncontrolled hypertension. Informed consent was obtained from all subjects following discussion of the study methodology and associated risks and benefits. In subjects where both eyes fit the inclusion and exclusion criteria, a single eye was selected at random for imaging. In order to correct for individual retinal magnification, axial lengths were measured using an IOL Master (Carl Zeiss Meditec, Inc., Dublin, CA).[52] Wide-field color fundus photography (Topcon 3D OCT 2000, Topcon Corporation, Tokyo, Japan) was performed on all NPDR subjects on the day of OCTA imaging. An in-house retina specialist (RBR) classified the NPDR eyes into mild, moderate, and severe disease according to the Early Treatment of Diabetic Retinopathy Study (ETDRS) system[23,53] by analyzing the color fundus photographs in conjunction with corresponding IVFA images if available within 6 months of image acquisition.

## OCTA and En Face OCT Reflectance Image Acquisition

All subjects were imaged using a commercial spectral domain OCT system (Avanti RTVue-XR; AngioVue version 2015.100.0.35; Optovue, Fremont, CA). Ten sequential 10×10° (~3×3 mm) macular scans were obtained in each subject,[49,54] and OCTA images were generated from the split-spectrum amplitude decorrelation angiography (SSADA) algorithm.[49,55,56] The retinal blood vessels were automatically separated into the superficial and deep layers for each scan. The superficial OCTA images included blood vessels from the inner limiting membrane

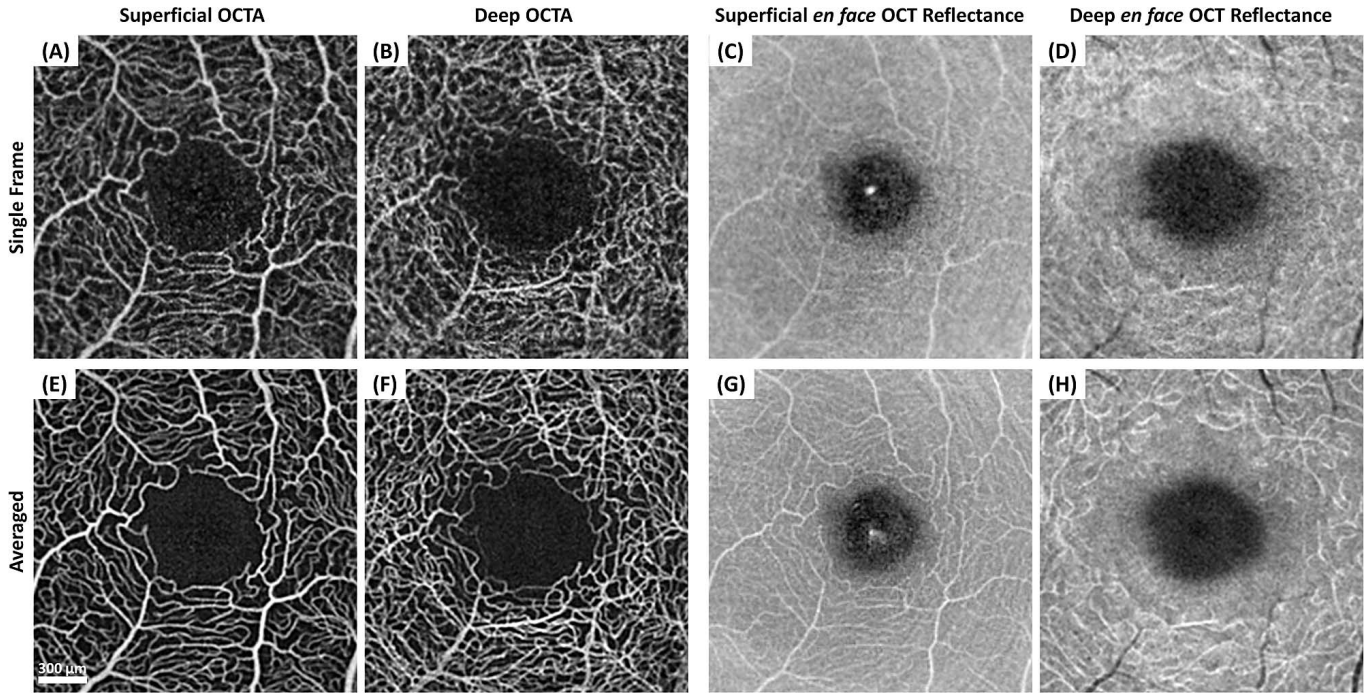


**Figure 1.** (A-D) Single-frame and (E-H) averaged OCTA and en face OCT reflectance images in a control subject. Averaging minimizes motion artifacts and provides clearer delineation of individual capillaries on both OCTA and en face OCT reflectance images.

(ILM) to 15 µm below the posterior boundary of the inner plexiform layer (IPL), whereas the deep OCTA images included blood vessels from 15 µm below the posterior boundary of the IPL to 70 µm below the posterior boundary of the IPL (Figs. 1A and 1B). Corresponding en face OCT reflectance images were also generated using the mean projection of the reflectance signal (Figs. 1C and 1D).

## Image Processing

### Image Registration and Averaging

In order to increase the signal-to-noise ratio and eliminate artifactual discontinuities in blood vessel segments that are often present on single-frame images,[57,58] we created averaged images for better segmentation and more accurate delineation of the FAZ and PICAs. For each set of 10 superficial OCTA images, a reference image with the highest contrast and least motion artifact was selected manually by an expert observer (BDK). The remaining superficial OCTA images were registered to this reference image using the Register Virtual Stack Slices plug-in on ImageJ (ImageJ, U.S. National Institutes of Health, Bethesda, MD);[59] we employed a rigid extraction model with elastic bUnwarpJ splines registration.[60] These same transformations were applied to the sets of deep OCTA, superficial en face OCT reflectance, and deep en face OCT reflectance images using the Transform Virtual Stack Slices plug-in on ImageJ, which were then averaged as well (Figs. 1E–1H). Differences between single and averaged images are demonstrated in Figure 1.

### Superficial OCTA Image Processing and Data Extraction

*Thresholding*. Using custom software on MATLAB (MathWorks, Natick, MA), the averaged superficial OCTA images were contrast stretched (Fig. 2A), and local thresholding was performed to convert the contrast-stretched grayscale OCTA images into binary images (Fig. 2B).[61] Only the threshold superficial OCTA images were used for FAZ and PICA analysis, as the deep layer is subject to projection artifacts that inhibit accurate blood vessel analysis.[58]

*FAZ and PICA Measurement and Creation of Reference Database*. On the threshold superficial OCTA images, the FAZ and all surrounding PICAs were automatically delineated using MATLAB (MathWorks) (Fig. 2C). FAZ area, perimeter, and acircularity index were computed using MATLAB's (MathWorks) regionprops function. Acircularity index was defined as the ratio of the perimeter of the FAZ to the perimeter of a circle with equal area.[62,63]

For each individual PICA, area, minor axis, and

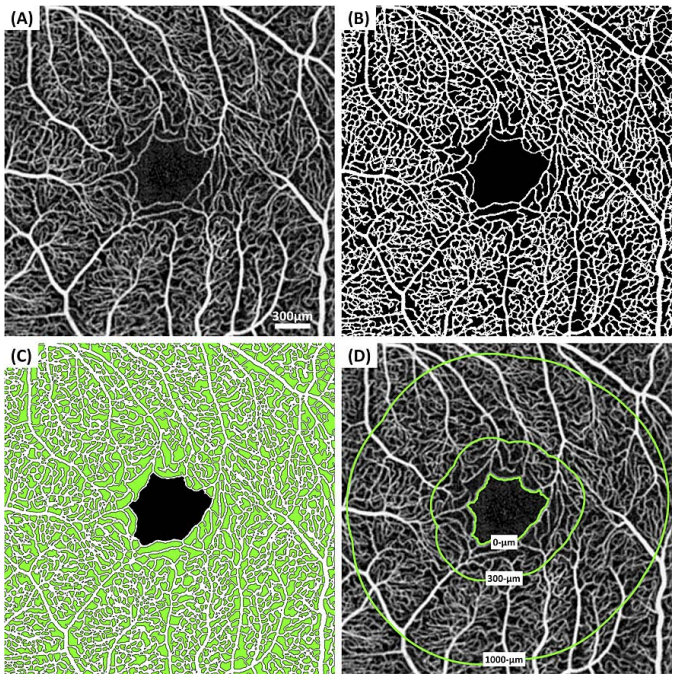


**Figure 2.** (A) Averaged superficial OCTA, (B) thresholded image, (C) automatic segmentation of FAZ (*black region*) and PICAs (*green regions*), and (D) creation of equal distance annuli of increasing retinal eccentricity from the FAZ margin with a 100-µm step size using distance transformation. *Green lines* represent 300-µm and 1000-µm ROIs from the FAZ margin, which is labeled as 0-µm for reference.

centroid location were computed using MATLAB's regionprops function. The minor axis was extracted from a best-fit ellipse generated from second order moments, and the centroid was defined as the center of mass.[64] Distance transformation was employed to create 12 consecutive equal distance annuli of increasing retinal eccentricity from the FAZ margin with a 100-µm step size (Fig. 2D). Based on the location of its centroid, each PICA was classified as being in a particular annulus. From the 19 control subjects, a reference database of PICAs was generated based on mean area and minor axis within each annulus.

*SD Categorization of PICA and SD Mapping*. For every subject within each of the four groups (control, noDR, NPDR, and PDR), each PICA delineated on the threshold superficial OCTA image was compared to the mean PICA area and minor axis of the reference database. PICAs were classified as nonperfused areas if they were $\geq$2 SDs above the mean area and minor axis at the corresponding annuli, and they were further grouped according to specific size: 2 to 3.9 SDs (cyan), 4 to 7.9 SDs (yellow), or $\geq$8 SDs (red) compared to the reference means. This color coding system was overlaid upon the averaged superficial OCTA image to create a SD map for each subject (Fig. 3, bottom row). For qualitative comparison, a color-coded vascular perfusion density map was generated from the thresholded image using an algorithm previously described (Fig.e 3, top row).[61,65]

*Calculation of Percent Nonperfused Area*. On the threshold superficial OCTA images, two regions of interest (ROI) were analyzed. The ROIs were defined as concentric rings with the inner border at the FAZ margin and the outer border at 300 µm and 1000 µm from the FAZ, respectively (Fig. 4). For each ROI, percent nonperfused area was calculated as the summed nonperfused areas divided by the total area of the ROI.

*Identification of Intermittent Flow*. After image registration, the single-frame superficial OCTA images were examined in sequence to identify intermittent flow. Intermittent flow was defined as the presence of a perfused blood vessel that was present on some but not all frames.

### Superficial En Face OCT Reflectance Image Processing

*Identification of Nonperfused Blood Vessel Segments*. The en face OCT reflectance images can provide additional information about blood vessel structure. Examining these images alongside the OCTA images can help identify nonperfused capillaries.[66] Each averaged, contrast-inverted superficial en face OCT reflectance image was overlaid on the corresponding averaged OCTA image using Adobe Photoshop CS6 (Adobe Systems, Inc., San Jose, CA). A nonperfused blood vessel segment was identified as a hyporeflective cord-like structure on the superficial en face OCT reflectance image that did not enhance on either the superficial or deep OCTA images.[66] An expert grader (BDK) counted the number of nonperfused blood vessel segments for each subject. For simplification, the regions where blood vessels were counted for data analysis included only the FAZ on the superficial OCTA image and the intercapillary areas contiguous with the FAZ.

## Statistical Analysis

Given that not all subgroups met the Anderson-Darling test for normality, values for FAZ metrics, percent nonperfused area, and number of nonperfused blood vessel segments identified on the superficial en face OCT reflectance images were compared

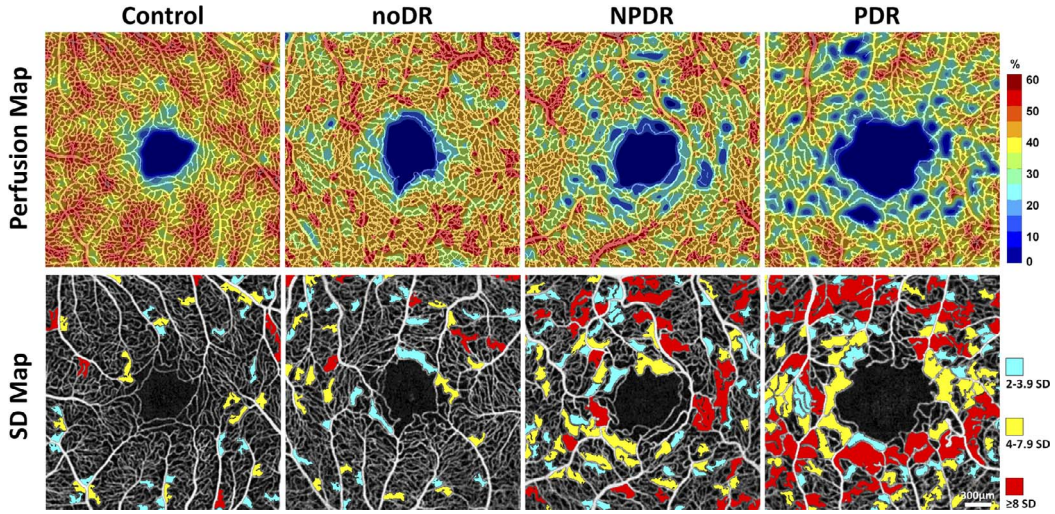


**Figure 3.** Perfusion maps (*top row*) and SD mapping of nonperfused areas (*bottom row*) overlaid with the superficial OCTA images from each group. Total percent nonperfused area (≥2 SDs) increases with worsening diabetic retinopathy, as seen by the increased prevalence of *red* and *yellow shaded regions* moving left to right in the SD maps.

between groups using the nonparametric Kruskal-Wallis and post-hoc Mann-Whitney *U* tests with the Holm-Bonferroni correction for multiple comparisons. For the reference PICA data from the controls, 95% confidence intervals were generated for area and minor axis at each 100-µm width annulus. The diagnostic capability of percent nonperfused area to differentiate between eyes with diabetic retinopathy (NPDR + PDR) and eyes without diabetic retinopathy (control + noDR) was assessed using area under the receiver operating characteristic curve (AROC), sensitivity at 95% specificity, and specificity at 95% sensitivity. Finally, the $\chi^2$ test with the Marascuilo procedure was used to compare the percentage of subjects within each group that had at least one nonperfused blood vessel segment identified on the superficial en face reflectance images. Statistical analysis was performed using Microsoft Excel (Microsoft Corporation, Redmond, WA) and R (R Foundation for Statistical Computing, Vienna, Austria).

# Results

## Subject Information

Demographic data is displayed in Table 1. In the NPDR group, 9 eyes were classified as mild, 3 as moderate, and 3 as severe. There were no significant differences in age between the 4 study groups ($P > 0.05$).

## FAZ Metrics

Boxplots of FAZ metrics are shown in Figure 5 with corresponding *P*-values between groups in Table

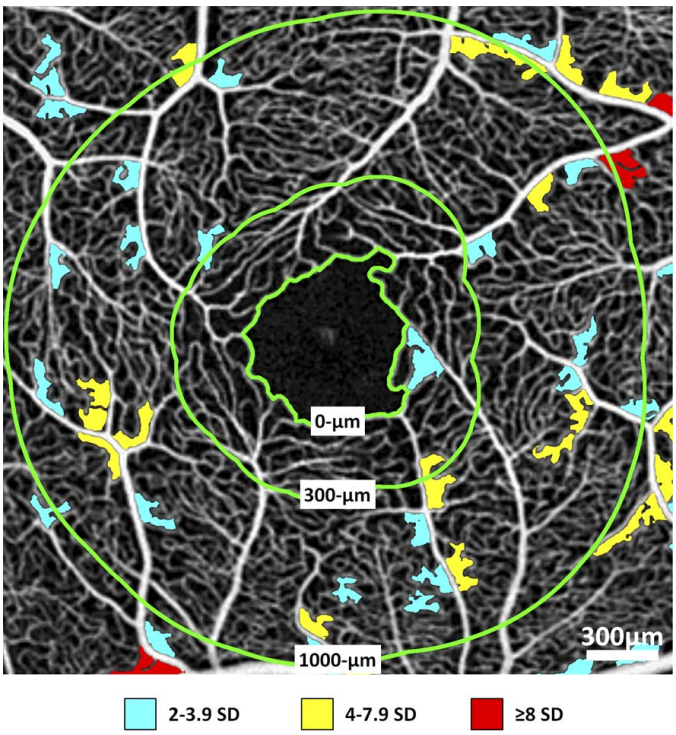


**Figure 4.** Computation of percent nonperfused area within 300-µm and 1000-µm ROIs in a control subject. SD map of nonperfused areas (*cyan*, *yellow*, and *red*) with overlying ROIs. Percent nonperfused area was calculated as the sum of the nonperfused areas within the ROI divided by the total area of the ROI.

**Table 1.** Demographic Data

| | Right/Left (*N*) | Type 1/Type 2 DM (*N*) | Male (%) | Age (Mean Years ± SD) | Previous Treatment Status (N) | | |
|---|---|---|---|---|---|---|---|
| | | | | | Treatment Naive | PRP Only | PRP + Anti-VEGF |
| Control | 15/4 | - | 42.1 | 51.9 ± 9.2 | - | - | - |
| noDR | 9/6 | 1/14 | 86.7 | 54.7 ± 10.8 | - | - | - |
| NPDR | 7/8 | 2/13 | 33.3 | 54.0 ± 8.2 | 14 | 1 | 0 |
| PDR | 7/8 | 3/12 | 60.0 | 46.9 ± 8.7 | 2 | 10 | 3 |

DM, diabetes mellitus; PRP, pan-retinal photocoagulation; anti-VEGF, anti-vascular endothelial growth factor injection.

2. Median and mean values are displayed in Supplementary Table S1. FAZ area was significantly greater in the NPDR and PDR groups compared to the control group. FAZ perimeter was significantly greater in the PDR group compared to the control and noDR groups, and it was also greater in the NPDR group compared to the control group. Acircularity index was significantly greater in the PDR group compared to the control and noDR groups. There were no significant differences observed between the control and noDR groups.

## PICA Metrics

Mean values for area and minor axis of the PICAs in the control group at increasing retinal eccentricities are displayed in Figure 6 with corresponding 95% confidence intervals. Mean area and minor axis at 100 μm from the FAZ margin were 5879 $\mu m^2$ and 56.0 μm, respectively. As expected, these values decreased with increasing annular distance, plateauing at approximately 600 μm from the FAZ margin.

## Percent Nonperfused Area

Median values ± interquartile range (IQR) for total percent nonperfused area (≥2 SDs) at the 300-μm ROI were 2.09 ± 4.42, 2.44 ± 4.75, 18.08 ± 17.27, and 27.55 ± 20.28 in the control, noDR, NPDR, and PDR groups, respectively. Median ± IQR at the 1000-μm ROI were 3.10 ± 2.26, 3.31 ± 3.74, 13.42 ± 12.76, and 23.00 ± 11.39. Histograms of total percent nonperfused area as well as cyan (2–3.9 SDs), yellow (4–7.9 SDs), and red (≥8 SDs) areas are shown in Figure 7, with corresponding *P*-values between groups in Table 2. Median and mean values are displayed in Supplementary Table S1. While there were no significant differences observed between the control and noDR groups, there was significantly greater percent nonperfused area in the NPDR and PDR groups versus the control and noDR groups for all other comparisons. Additionally, values were significantly greater in the PDR group compared to the NPDR group for the total percent nonperfused area and yellow area in the 300-μm ROI, and for the total percent nonperfused area, yellow area, and red area in the 1000-μm ROI.

The results of the receiver operating characteristic (ROC) curve analyses for percent nonperfused areas are displayed in Table 3. In distinguishing between eyes with diabetic retinopathy and eyes without diabetic retinopathy, the red (≥8 SDs) area at the 1000-μm ROI yielded the greatest AROC (0.99), sensitivity at 95% specificity (93.3%), and specificity at 95% sensitivity (94.1%).

## Identification of Intermittent Flow

Intermittent flow was identified in 4 eyes. All of these eyes had PDR (see Supplementary Video S1 showing registered superficial OCTA images in sequence in an eye with PDR, with arrows indicating blood vessels that enhance on some but not all of the single-frame OCTA images). There was no intermittent flow detected in the control, noDR, or NPDR groups.

## Identification of Nonperfused Blood Vessel Segments

The median ± IQR of nonperfused blood vessel segments identified on the superficial en face OCT reflectance images was 0.0 ± 1.0, 0.0 ± 1.0, 4.0 ± 7.0, and 8.0 ± 6.0 for the control, noDR, NPDR, and PDR groups, respectively. Mean ± SD was 0.63 ± 1.01, 0.73 ± 0.96, 4.73 ± 4.57, and 10.13 ± 9.31. Significant differences were observed for all comparisons except between the control and noDR groups (Table 2). The percentage of eyes having at least one identified nonperfused segment was 42% in the control group, 47% in the noDR group, 93% in the NPDR group, and 100% in the PDR group. Using the

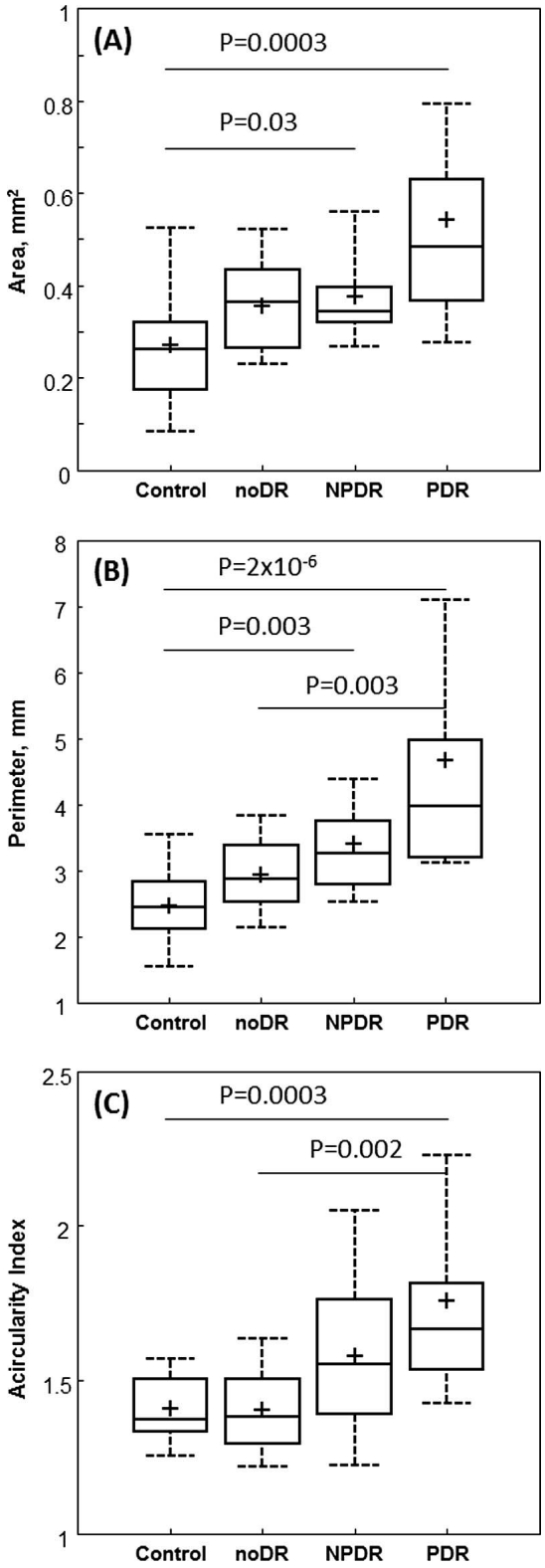


Figure 5. Boxplots of FAZ metrics. (A) FAZ area, (B) FAZ perimeter, and (C) FAZ acircularity showing means (*cross*), medians (*horizontal lines*), 25%-75% quartiles (*boxes*), and 9%–91% percentile ranges (*whiskers*). Significant *P*-values for the post-hoc pairwise comparisons after nonparametric Kruskal-Wallis tests are shown; all other comparisons were not significant ($P > 0.05$).

$\chi^2$ test followed by the Marascuilo procedure at a 0.05 level of significance, this percentage was significantly different for the NPDR verses control, NPDR verses noDR, PDR verses control, and PDR verses noDR comparisons. Figure 8 demonstrates nonperfused blood vessel segments in an eye with NPDR.

## Discussion

Macular nonperfusion is an important cause of visual loss in patients with DR, and it has been shown to be a risk factor for progression to more advanced disease.[1–11,19] Hence, there is an ostensible need for a technique to reliably quantify these microvascular changes. We have demonstrated a unique image processing and mapping technique that can measure parafoveal nonperfusion, showing promise as an approach to assess disease.

The study's results for FAZ metrics measured in the control and diabetic groups were within the ranges of values reported in previous studies on FAZ geometry.[24,26,29,42,43,45,63] Although these metrics generally showed stepwise increases in values with worsening retinopathy, the study's findings of few significant differences between groups confirmed the existence of substantial variability in the FAZ for both controls and diabetics, and the difficulty of using these metrics alone to separate different stages of disease.

PICAs are known to decrease in size with increasing eccentricity from the FAZ in healthy retinas,[67] and the study's findings of PICA area and minor axis (Fig. 6) corroborated this finding. This observation supports the notion that with increasing inner retinal thickness further away from the foveal center, there are more vascular branches in a 3-dimensional configuration to effectively nourish larger volumes of tissue.[68–71] As a result, it was critical to make the database retinal eccentricity–specific. Overall, the study's area values for normal PICAs were consistent with those reported previously.[29,30,67,72,73] Additionally, the study's mean minor axis values agreed with earlier reports that demonstrate the optimal intercapillary distance to supply the surrounding retinal ganglion cells and axons.[68,71,74,75] Specifically, the mean minor axis measured at the 100-µm annulus should closely reflect the maximal intercapillary distance for optimal diffusion, as the superficial capillary network directly bordering the FAZ is single-layered.[71,76,77] The study's value of 56-µm closely aligns with previous work suggesting that this value is around 60-µm.[68] This is one reason why

**Table 2.** *P*-Values Between Groups for FAZ Metrics, Percent Nonperfused Area, and Number of Identified Nonperfused Blood Vessel Segments

| | | Control v. noDR | Control v. NPDR | Control v. PDR | noDR v. NPDR | noDR v. PDR | NPDR v. PDR |
|---|---|---|---|---|---|---|---|
| FAZ metrics | Area | 0.08 | 0.03* | 0.0003* | 0.7 | 0.06 | 0.08 |
| | Perimeter | 0.08 | 0.003* | $2\times10^{-6}$* | 0.1 | 0.003* | 0.08 |
| | Acircularity index | 0.8 | 0.2 | 0.0003* | 0.3 | 0.002* | 0.3 |
| Nonperfused area, 300-μm ROI | ≥2 SD | 0.6 | $7\times10^{-5}$* | $7\times10^{-6}$* | 0.0001* | $2\times10^{-5}$* | 0.04* |
| | 2-3.9 SD | 0.3 | 0.007* | 0.007* | 0.04* | 0.03* | 0.8 |
| | 4-7.9 SD | 0.9 | 0.02* | 0.0001* | 0.01* | 0.0003* | 0.02* |
| | ≥8 SD | 0.7 | $4\times10^{-5}$* | $2\times10^{-6}$* | $6\times10^{-5}$* | $6\times10^{-6}$* | 0.06 |
| Nonperfused area, 1000-μm ROI | ≥2 SD | 0.6 | $2\times10^{-6}$* | $7\times10^{-9}$* | $6\times10^{-5}$* | $6\times10^{-8}$* | 0.01* |
| | 2-3.9 SD | 0.8 | 0.0001* | $7\times10^{-6}$* | 0.0004* | $2\times10^{-6}$* | 0.8 |
| | 4-7.9 SD | 0.3 | $5\times10^{-5}$* | $3\times10^{-8}$* | 0.0007* | $6\times10^{-8}$* | 0.002* |
| | ≥8 SD | 0.6 | $5\times10^{-6}$* | $5\times10^{-6}$* | $5\times10^{-5}$* | $1\times10^{-5}$* | 0.02* |
| Nonperfused blood vessel segments | | 0.7 | 0.002* | $7\times10^{-6}$* | 0.007* | $4\times10^{-5}$* | 0.04* |

* Indicates $P < 0.05$.

we included minor axis in combination with area as a metric to separate normal from abnormally large PICAs, as area alone cannot accurately separate healthy retina from ischemic regions, especially for slender and elongated PICAs with above-mean PICA area that still maintain acceptable intercapillary distances for nutrient diffusion. These elongated PICAs are especially prominent adjacent to retinal arteries, known as periarteriolar capillary free zones.[78,79] Hence, minor axis can be used as an adjunct to area when categorizing PICA size.

Prior studies have used OCTA to quantify perfusion deficits in DR by measuring perfusion density.[43,49,50] However, this metric is limited in its ability to detect finite areas of abnormal perfusion due to the difficulties of creating a reference database. Aside from the increase in perfusion density at greater distances from the FAZ, the obstacles to creating such a database stem from variations in major blood vessel patterns in normal individuals, which make it challenging to define a reference perfusion density value at a particular location in the macula. Newer approaches have quantified these changes at the macula by measuring an aggregate nonperfused area, showing overall enlargement in DR when compared to controls.[43,46,47,80] This type of analysis represents an inverse to perfusion density. This method goes one step further by creating an eccentricity-specific reference database, making it possible to detect finite perfusion deficits as well.

There have been few attempts to quantify individual PICAs that may suggest focal ischemia; Schottenhamml et al. demarcated all PICAs in diabetics and controls using a custom automatic algorithm, demonstrating a stepwise increase in the mean of the 10 and 20 largest PICAs with worsening severity of retinopathy.[48] Their findings illustrate the potential for classifying individual PICAs based on size. We have expanded upon this idea by categorizing PICAs according to SD thresholds and highlighting regions with nonperfusion. The study's results showing an increase in percent nonperfused area from subjects without retinopathy (control + noDR) to NPDR and finally PDR, with significant differences observed between nearly all groups for all comparisons, suggest that this method can be used to accurately quantify global nonperfusion using different thresholds to help assess disease severity. Additionally, AROC values for percent nonperfused area demonstrated very good (>0.8)[81] diagnostic accuracy for all thresholds when differentiating between eyes with and without diabetic retinopathy. The red (≥8 SDs) area at the 1000-μm ROI demonstrated the greatest AROC, sensitivity at 95% specificity, and specificity at 95% sensitivity, suggesting that measuring larger areas may exhibit greater capability to distinguish between eyes with and without disease. The combination of numerical and visual information that can measure global nonperfusion as well as identify focal defects can be helpful in clinical practice and may be especially useful when monitoring disease progression or response to treatment. Of particular interest are

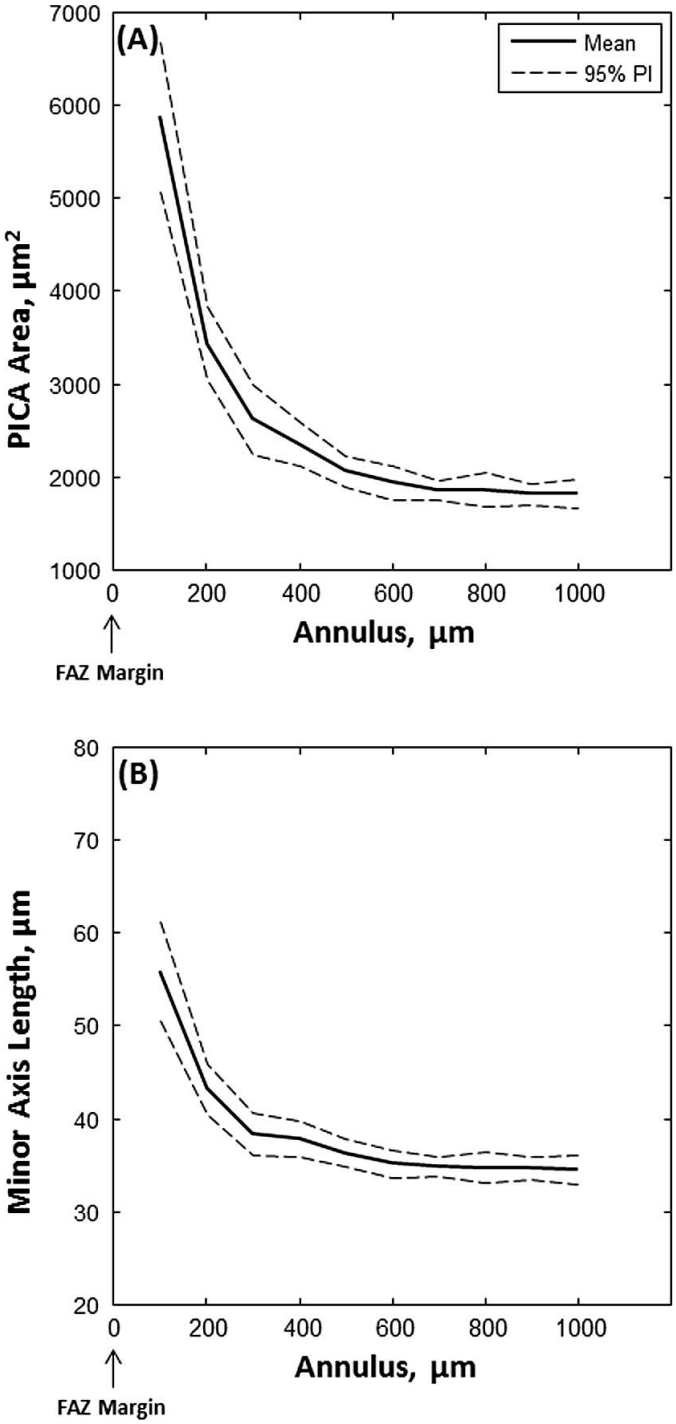


Figure 6. PICA data from the control group. (A) mean area of PICAs and (B) mean minor axis at increasing annular distance from the FAZ margin. *Dashed lines* represent 95% confidence intervals for each metric.

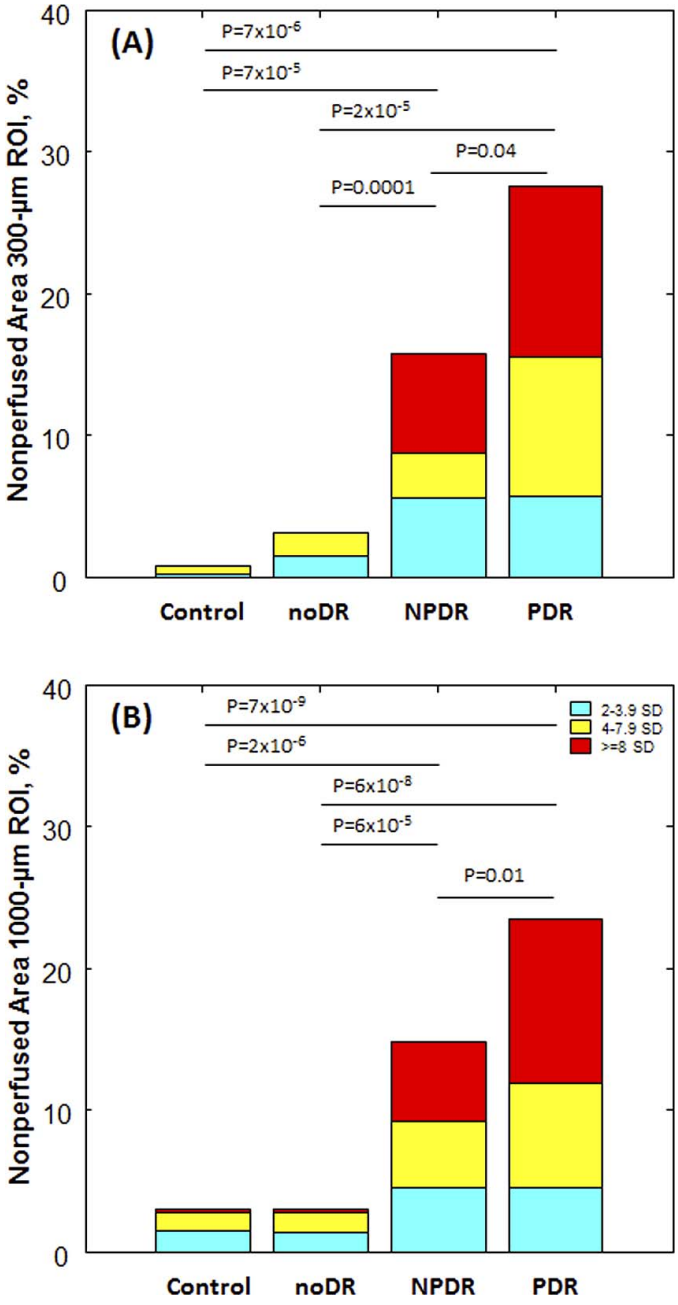


Figure 7. Stacked histograms of median percent nonperfused area for the (A) 300-µm and (B) 1000-µm ROIs. Significant *P*-values for the post-hoc pairwise comparisons after nonparametric Kruskal-Wallis tests are shown for the total percent nonperfused area (≥2 SDs). Only the control versus noDR comparisons were not significant ($P > 0.05$). Sub-analyses of 2 to 3.9 SDs, 4 to 7.9 SDs, and ≥8 SDs are provided in Table 2.

longitudinal studies showing changes over time in percent nonperfused area as well as in size of discrete PICAs.

The study's OCTA image averaging technique, first described by Mo et al.,[57] offers several advantages. It increases the signal-to-noise ratio, helping remove motion artifacts and false discontinuities in blood vessels from single-frame OCTA images, enabling automatic and reliable segmentation of the

**Table 3.** ROC Curve Analyses of Percent Nonperfused Area Between Eyes With Diabetic Retinopathy (NPDR + PDR) and Eyes Without Diabetic Retinopathy (Control + noDR). 95% Confidence Intervals Are Included in Parentheses

| | | Area Under Curve | Sensitivity (at 95% Specificity) | Specificity (at 95% Sensitivity) |
|---|---|---|---|---|
| 300-μm ROI | ≥2 SD | 0.97 (0.93–1) | 86.7 (60.0–96.7) | 79.4 (50.0–100) |
| | 2 to 3.9 SD | 0.81 (0.70–0.91) | 43.3 (0.0–70.0) | 35.2 (13.2–67.7) |
| | 4 to 7.9 SD | 0.86 (0.77–0.95) | 60.0 (40.0–76.8) | 41.2 (23.5–64.7) |
| | ≥8 SD | 0.95 (0.90–1) | 86.7 (63.3–100) | 70.6 (27.4–100) |
| 1000-μm ROI | ≥2 SD | 0.97 (0.93–1) | 86.7 (70.0–96.7) | 82.4 (41.2–100) |
| | 2 to 3.9 SD | 0.92 (0.85–0.99) | 66.7 (0.0–90.0) | 73.5 (38.2–91.2) |
| | 4 to 7.9 SD | 0.95 (0.89–1) | 80.0 (53.3–96.7) | 58.8 (23.5–97.1) |
| | ≥8 SD | 0.99 (0.98–1) | 93.3 (83.3–100) | 94.1 (79.4–100) |

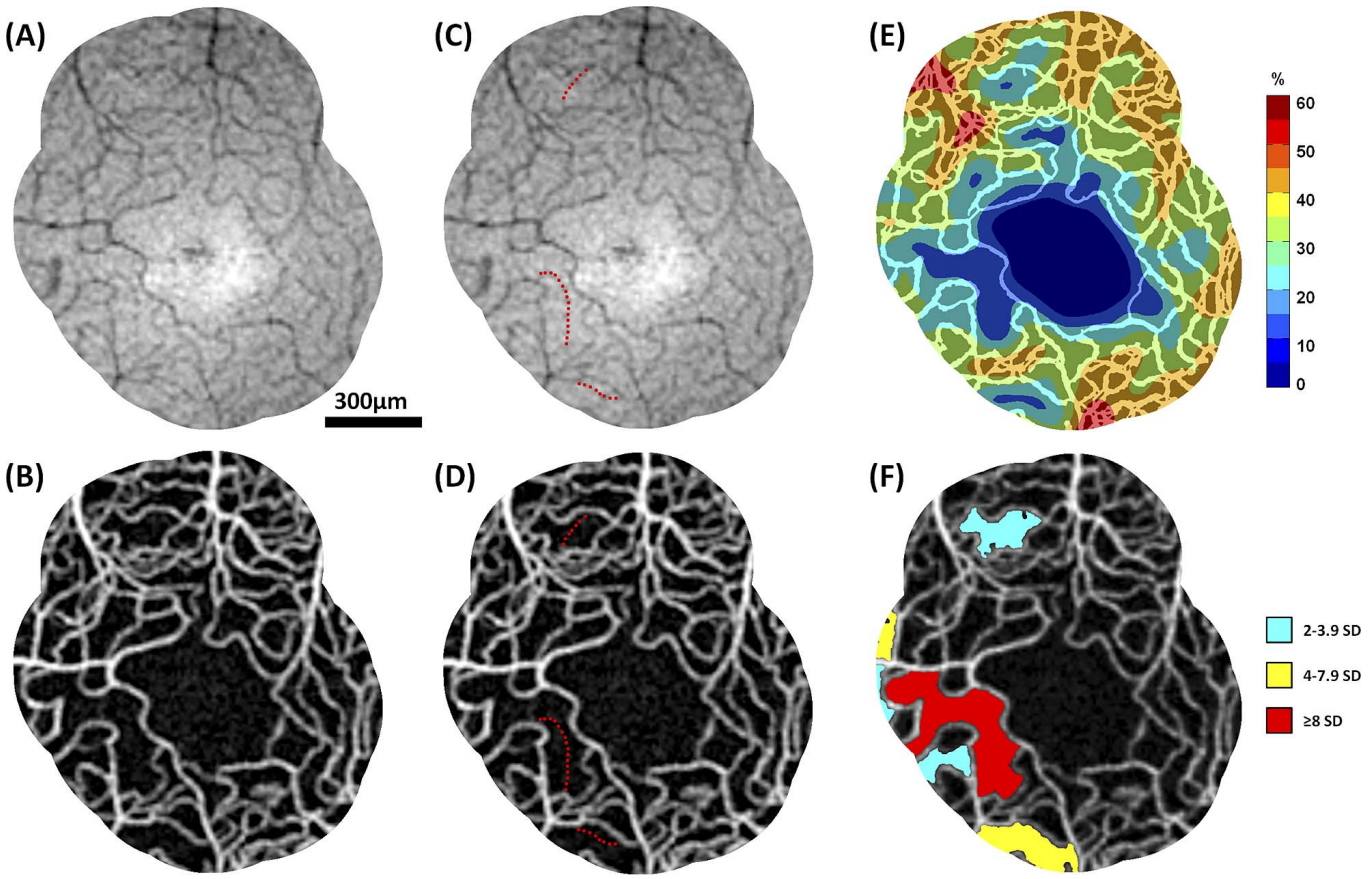


**Figure 8.** Identification of nonperfused blood vessel segments in a subject with NPDR. (A) averaged and contrast-inverted superficial en face OCT reflectance image with corresponding averaged superficial OCTA image (B). (C and D) averaged superficial en face OCT reflectance and superficial OCTA images with nonperfused blood vessel segments *demarcated in red*; these segments appear as hyporeflective cord-like structures on the OCT reflectance image but do not enhance on the OCTA image. (E and F) Corresponding perfusion density map and SD map of nonperfused areas. Locations with lower perfusion density and nonperfused areas correspond to the locations of nonperfused blood vessels.

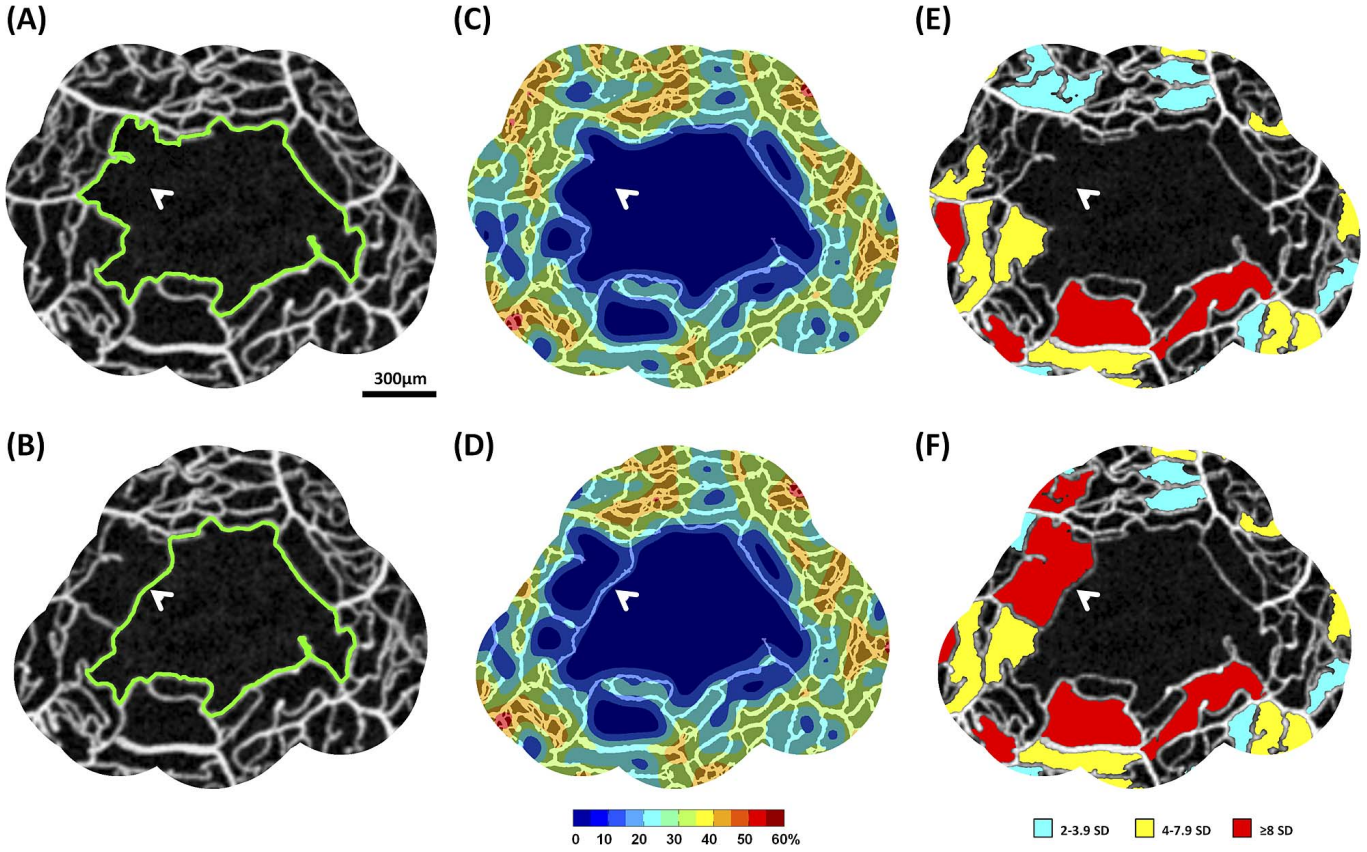


**Figure 9.** Effect of intermittent flow on SD mapping. (A and B) superficial OCTA images on the same PDR subject with intermittent flow (*arrows*) occurring at the FAZ margin (*green*). Both panels show the 300-µm ROI from the FAZ margin. (C and D) corresponding perfusion density maps and (E and F) SD maps of nonperfused areas. Identification of nonperfused areas within the 300-µm ROI changes with the variation of the FAZ margin, leading to different appearances of the SD maps on the same subject.

FAZ and surrounding PICAs. Additionally, coregistration of the en face OCT reflectance images provides additional information about vascular structure. Figure 8 demonstrates the ability to localize blood vessels that are present on the superficial en face OCT reflectance images but absent from the OCTA images, which likely represent nonperfused capillaries.[66] The locations of nonperfused segments correspond well to the nonperfused areas in this subject. The presence of intact vascular structure on the en face OCT reflectance image that does not enhance on OCTA suggests that these vessels may have the potential to recanalize,[66,82] which can help predict the potential benefits of interventions to improve macular perfusion[83] and monitor the response on a structural level. Furthermore, the ability to identify blood vessels with intermittent flow (Supplementary Video S1) while viewing single-frame OCTA images in sequence offers another method for detecting focal blood vessel defects. It is possible that these vessels undergoing transient occlusion of their lumens are at higher risk for complete occlusion.

We were unable to show differences between the control and noDR groups for any comparisons. However, both control and noDR subjects exhibited some nonperfused areas (Fig. 3). While these findings may simply be due to normal variation, larger (i.e., $\geq$8 SDs) areas may indicate subclinical ischemia. Perhaps these regions should be monitored closely for progression, even in patients with no discernible vascular disease, as areas with capillary occlusion may be susceptible to further dropout.[84] The fact that several control subjects (42%) exhibited nonperfused capillaries on en face OCT reflectance images suggests that there are changes in vascular perfusion that occur even in healthy eyes.[85]

There are several limitations to this study. While we have referred to the cord-like structures on en face OCT reflectance images that do not enhance on OCTA as nonperfused blood vessel segments, these segments may actually reflect slow blood flow rather

than total obstruction.[5,9,29,30,86–88] Given that the detection velocity threshold on OCTA is 0.3 mm/s,[89] this modality has the potential to ignore blood vessels with very slow flow. Regardless of the exact processes at play, capillary occlusion and slow flow all indicate hypoperfusion and put the retina at risk for ischemic damage, and identification of these regions is critical. Additionally, if intermittent flow occurs at the FAZ margin, the FAZ margin and the subsequent annulus locations for PICA distribution can change, making it possible for a single eye to have different appearances of the SD maps at consecutive time points (Fig. 9). Other limitations include small sample size and strict inclusion criteria. We also only studied the superficial capillary layer, as accurate analysis of the deep layer is limited by projection artifacts.[58] As such, it is difficult to generalize the study's results to the deeper capillary layers.

In summary, we have demonstrated a novel technique to quantify parafoveal nonperfusion in DR that is noninvasive, automatic, and retinal eccentricity–specific. It provides comprehensive analysis of parafoveal nonperfusion as well as information about individual defects. This method can help assess disease severity and shows promise as an approach to detect progression and treatment response over time at both the global and focal level.

## Acknowledgments

The authors thank Rachel Linderman for help recruiting and imaging some of the subjects. The authors also thank Jorge S. Andrade Romo for assistance with chart and image review.

This study was presented in part at the Association for Research in Vision and Ophthalmology Conference in May 2017: Rosen RB, Krawitz B, Philips E, Bavier R, Mo S, Weitz R, Carroll J, Chui T. Anatomical Location-Specific Normative Quantification of Macular Nonperfusion in Diabetic Retinopathy using Optical Coherence Tomography Angiography (OCTA).

**Grant Information:** Supported by the National Eye Institute of the National Institutes of Health under award numbers R01EY027301, R01EY024969, and P30EY001931. The content is solely the responsibility of the authors and does not necessarily represent the official views of the National Institutes of Health. Additional funding for this research was provided by the New York Eye and Ear Infirmary Foundation Grant, the Marrus Family Foundation, and the Geraldine Violett Foundation. The sponsors and funding organizations had no role in the design or conduct of this research.

Disclosure: **B.D. Krawitz,** None; **E. Phillips,** None; **R.D. Bavier,** None; **S. Mo,** None; **J. Carroll,** (F); **R.B. Rosen,** (I, C); **T.Y.P. Chui,** None

## References

1. Bresnick GH, De Venecia G, Myers FL, Harris JA, Davis MD. Retinal ischemia in diabetic retinopathy. *Arch Ophthalmol*. 1975;93:1300–1310.
2. Klein R, Klein BE, Moss SE. Visual impairment in diabetes. *Ophthalmology*. 1984;91:1–9.
3. Aiello LP, Wong JS. Role of vascular endothelial growth factor in diabetic vascular complications. *Kidney Int Suppl*. 2000;77:S113–119.
4. Grant MB, Afzal A, Spoerri P, Pan H, Shaw LC, Mames RN. The role of growth factors in the pathogenesis of diabetic retinopathy. *Expert Opin Investig Drugs*. 2004;13:1275–1293.
5. Sakata K, Funatsu H, Harino S, Noma H, Hori S. Relationship of macular microcirculation and retinal thickness with visual acuity in diabetic macular edema. *Ophthalmology*. 2007;114:2061–2069.
6. Unoki N, Nishijima K, Sakamoto A, et al. Retinal sensitivity loss and structural disturbance in areas of capillary nonperfusion of eyes with diabetic retinopathy. *Am J Ophthalmol*. 2007;144:755–760.
7. Sim DA, Keane PA, Fung S, et al. Quantitative analysis of diabetic macular ischemia using optical coherence tomography. *Invest Ophthalmol Vis Sci*. 2014;55:417–423.
8. Arend O, Remky A, Evans D, Stüber R, Harris A. Contrast sensitivity loss is coupled with capillary dropout in patients with diabetes. *Invest Ophthalmol Vis Sci*. 1997;38:1819–1824.
9. Arend O, Wolf S, Harris A, Reim M. The relationship of macular microcirculation to visual acuity in diabetic patients. *Arch Ophthalmol*. 1995;113:610–614.
10. Sim DA, Keane PA, Zarranz-Ventura J, et al. The effects of macular ischemia on visual acuity in diabetic retinopathy. *Invest Ophthalmol Vis Sci*. 2013;54:2353–2360.

11. Fluorescein angiographic risk factors for progression of diabetic retinopathy. ETDRS report number 13. Early Treatment Diabetic Retinopathy Study Research Group. *Ophthalmology* 1991; 98:834–840.
12. McMillan DE. Plasma protein changes, blood viscosity, and diabetic microangiopathy. *Diabetes*. 1976;25:858–864.
13. McMillan DE, Utterback NG, La Puma J. Reduced erythrocyte deformability in diabetes. *Diabetes*. 1978;27:895–901.
14. Schmid-Schonbein H, Volger E. Red-cell aggregation and red-cell deformability in diabetes. *Diabetes*. 1976;25:897–902.
15. Sagel J, Colwell JA, Crook L, Laimins M. Increased platelet aggregation in early diabetus mellitus. *Ann Intern Med*. 1975;82:733–738.
16. Ernst E, Matrai A. Altered red and white blood cell rheology in type II diabetes. *Diabetes*. 1986; 35:1412–1415.
17. Schroder S, Palinski W, Schmid-Schonbein GW. Activated monocytes and granulocytes, capillary nonperfusion, and neovascularization in diabetic retinopathy. *Am J Pathol*. 1991;139:81–100.
18. Miyamoto K, Khosrof S, Bursell SE, et al. Prevention of leukostasis and vascular leakage in streptozotocin-induced diabetic retinopathy via intercellular adhesion molecule-1 inhibition. *Proc Natl Acad Sci U S A*. 1999;96:10836–10841.
19. Ip MS, Domalpally A, Sun JK, Ehrlich JS. Long-term effects of therapy with ranibizumab on diabetic retinopathy severity and baseline risk factors for worsening retinopathy. *Ophthalmology*. 2015;122:367–374.
20. Ticho U, Patz A. The role of capillary perfusion in the management of diabetic macular edema. *Am J Ophthalmol*. 1973;76:880–886.
21. Jonas JB, Martus P, Degenring RF, Kreissig I, Akkoyun I. Predictive factors for visual acuity after intravitreal triamcinolone treatment for diabetic macular edema. *Arch Ophthalmol*. 2005; 123:1338–1343.
22. Chung EJ, Roh MI, Kwon OW, Koh HJ. Effects of macular ischemia on the outcome of intravitreal bevacizumab therapy for diabetic macular edema. *Retina*. 2008;28:957–963.
23. Classification of diabetic retinopathy from fluorescein angiograms. ETDRS report number 11. Early Treatment Diabetic Retinopathy Study Research Group. *Ophthalmology*. 1991;98:807–822.
24. Bresnick GH, Condit R, Syrjala S, Palta M, Groo A, Korth K. Abnormalities of the foveal avascular zone in diabetic retinopathy. *Arch Ophthalmol*. 1984;102:1286–1293.
25. Mansour AM, Schachat A, Bodiford G, Haymond R. Foveal avascular zone in diabetes mellitus. *Retina*. 1993;13:125–128.
26. Conrath J, Giorgi R, Raccah D, Ridings B. Foveal avascular zone in diabetic retinopathy: quantitative vs qualitative assessment. *Eye (Lond)*. 2005;19:322–326.
27. Ffytche TJ, Shilling JS, Chisholm IH, Federman JL. Indications for fluorescein angiography in disease of the ocular fundus: a review. *J R Soc Med*. 1980;73:362–365.
28. Rabb MF, Burton TC, Schatz H, Yannuzzi LA. Fluorescein angiography of the fundus: a schematic approach to interpretation. *Surv Ophthalmol*. 1978;22:387–403.
29. Arend O, Wolf S, Jung F, et al. Retinal microcirculation in patients with diabetes mellitus: dynamic and morphological analysis of perifoveal capillary network. *Br J Ophthalmol*. 1991;75:514–518.
30. Arend O, Wolf S, Remky A, et al. Perifoveal microcirculation with non-insulin-dependent diabetes mellitus. *Graefes Arch Clin Exp Ophthalmol*. 1994;232:225–231.
31. Sleightholm MA, Aldington SJ, Arnold J, Kohner EM. Diabetic retinopathy: II. Assessment of severity and progression from fluorescein angiograms. *J Diabet Complications*. 1988;2:117–120.
32. Sander B, Larsen M, Engler C, Lund-Andersen H, Parving HH. Early changes in diabetic retinopathy: capillary loss and blood-retina barrier permeability in relation to metabolic control. *Acta Ophthalmol (Copenh)*. 1994;72:553–559.
33. Mendis KR, Balaratnasingam C, Yu P, et al. Correlation of histologic and clinical images to determine the diagnostic value of fluorescein angiography for studying retinal capillary detail. *Invest Ophthalmol Vis Sci*. 2010;51:5864–5869.
34. Zheng Y, Gandhi JS, Stangos AN, Campa C, Broadbent DM, Harding SP. Automated segmentation of foveal avascular zone in fundus fluorescein angiography. *Invest Ophthalmol Vis Sci*. 2010;51:3653–3659.
35. Johnson RN, Fu AD, McDonald HR, et al. Fluorescein angiography: basic principles and interpretation. In: Ryan SJ, Hinton DR, Sadda SVR, Wiedemann P, Schachat AP, Wilkinson CP, eds. *Retina*. Amsterdam, the Netherlands: Elsevier Health Sciences; 2013:2–50.
36. Hwang TS, Jia Y, Gao SS, et al. Optical coherence tomography angiography features of diabetic retinopathy. *Retina*. 2015;35:2371–2376.

37. Couturier A, Mane V, Bonnin S, et al. Capillary plexus anomalies in diabetic retinopathy on optical coherence tomography angiography. *Retina*. 2015;35:2384–2391.
38. Balbino M, Silva G, Correia GC. Anaphylaxis with convulsions following intravenous fluorescein angiography at an outpatient clinic. *Einstein (Sao Paulo)*. 2012;10:374–376.
39. Johnson RN, McDonald HR, Schatz H. Rash, fever, and chills after intravenous fluorescein angiography. *Am J Ophthalmol*. 1998;126:837–838.
40. Yannuzzi LA, Rohrer KT, Tindel LJ, et al. Fluorescein angiography complication survey. *Ophthalmology*. 1986;93:611–617.
41. Di G, Weihong Y, Xiao Z, et al. A morphological study of the foveal avascular zone in patients with diabetes mellitus using optical coherence tomography angiography. *Graefes Arch Clin Exp Ophthalmol*. 2016;254:873–879.
42. Freiberg FJ, Pfau M, Wons J, Wirth MA, Becker MD, Michels S. Optical coherence tomography angiography of the foveal avascular zone in diabetic retinopathy. *Graefes Arch Clin Exp Ophthalmol*. 2016;254:1051–1058.
43. Hwang TS, Gao SS, Liu L, et al. Automated quantification of capillary nonperfusion using optical coherence tomography angiography in diabetic retinopathy. *JAMA Ophthalmol*. 2016;134:367–373.
44. Kim DY, Fingler J, Zawadzki RJ, et al. Noninvasive imaging of the foveal avascular zone with high-speed, phase-variance optical coherence tomography. *Invest Ophthalmol Vis Sci*. 2012;53:85–92.
45. Takase N, Nozaki M, Kato A, Ozeki H, Yoshida M, Ogura Y. Enlargement of foveal avascular zone in diabetic eyes evaluated by en face optical coherence tomography angiography. *Retina*. 2015;35:2377–2383.
46. Ishibazawa A, Nagaoka T, Takahashi A, et al. Optical coherence tomography angiography in diabetic retinopathy: a prospective pilot study. *Am J Ophthalmol*. 2015;160:35–44.e31.
47. Salz DA, de Carlo TE, Adhi M, et al. Select features of diabetic retinopathy on swept-source optical coherence tomographic angiography compared with fluorescein angiography and normal eyes. *JAMA Ophthalmol*. 2016;134:644–650.
48. Schottenhamml J, Moult EM, Ploner S, et al. An automatic, intercapillary area-based algorithm for quantifying diabetes-related capillary dropout using optical coherence tomography angiography. *Retina*. 2016;36(suppl 1):S93–S101.
49. Agemy SA, Scripsema NK, Shah CM, et al. Retinal vascular perfusion density mapping using optical coherence tomography angiography in normals and diabetic retinopathy patients. *Retina*. 2015;35:2353–2363.
50. Bhanushali D, Anegondi N, Gadde SG, et al. Linking retinal microvasculature features with severity of diabetic retinopathy using optical coherence tomography angiography. *Invest Ophthalmol Vis Sci*. 2016;57:Oct519–525.
51. Chylack LT, Jr., Wolfe JK, Singer DM, et al. The lens opacities classification system III. The longitudinal study of cataract study group. *Arch Ophthalmol*. 1993;111:831–836.
52. Bennett AG, Rudnicka AR, Edgar DF. Improvements on Littmann's method of determining the size of retinal features by fundus photography. *Graefes Arch Clin Exp Ophthalmol*. 1994;232:361–367.
53. Grading diabetic retinopathy from stereoscopic color fundus photographs–an extension of the modified Airlie House classification. ETDRS report number 10. *Ophthalmology*. 1991;98:786–806.
54. Mo S, Krawitz B, Efstathiadis E, et al. Imaging foveal microvasculature: optical coherence tomography angiography versus adaptive optics scanning light ophthalmoscope fluorescein angiography. *Invest Ophthalmol Vis Sci*. 2016;57:Oct130–140.
55. Jia Y, Tan O, Tokayer J, et al. Split-spectrum amplitude-decorrelation angiography with optical coherence tomography. *Opt Express*. 2012;20:4710–4725.
56. Spaide RF, Klancnik JM, Jr., Cooney MJ. Retinal vascular layers imaged by fluorescein angiography and optical coherence tomography angiography. *JAMA Ophthalmol*. 2015;133:45–50.
57. Mo S, Phillips E, Krawitz BD, et al. Visualization of radial peripapillary capillaries using optical coherence tomography angiography: the effect of image averaging. *PLoS One*. 2017;12:e0169385.
58. Spaide RF, Fujimoto JG, Waheed NK. Image artifacts in optical coherence tomography angiography. *Retina*. 2015;35:2163–2180.
59. Schneider CA, Rasband WS, Eliceiri KW. NIH Image to ImageJ: 25 years of image analysis. *Nat Methods*. 2012;9:671–675.
60. Arganda-Carreras I, Sorzano COSS, Marabini R, Carazo JM, Ortiz-De-Solorzano C, Kybic J. Consistent and elastic registration of histological sections using vector-spline regularization. In: Beichel RR, Sonka M, eds. *Lecture Notes in*

*Computer Science*. Berlin-Heidelberg, Germany: Springer; 2006:85–95.
61. Scripsema NK, Garcia PM, Bavier RD, et al. Optical coherence tomography angiography analysis of perfused peripapillary capillaries in primary open-angle glaucoma and normal-tension glaucoma. *Invest Ophthalmol Vis Sci*. 2016;57: Oct611–Oct620.
62. Tam J, Dhamdhere KP, Tiruveedhula P, et al. Disruption of the retinal parafoveal capillary network in type 2 diabetes before the onset of diabetic retinopathy. *Invest Ophthalmol Vis Sci*. 2011;52:9257–9266.
63. Krawitz BD, Mo S, Geyman LS, et al. Acircularity index and axis ratio of the foveal avascular zone in diabetic eyes and healthy controls measured by optical coherence tomography angiography. *Vision Res* 2017;139:177–186.
64. Larson R, Hostetler RP, Edwards BH. *Calculus of a single variable*. 6 ed. Boston, MA: Houghton Mifflin; 1997.
65. Pinhas A, Dubow M, Shah N, et al. Fellow eye changes in patients with nonischemic central retinal vein occlusion: assessment of perfused foveal microvascular density and identification of nonperfused capillaries. *Retina*. 2015;35:2028–2036.
66. Miwa Y, Murakami T, Suzuma K, et al. Relationship between functional and structural changes in diabetic vessels in optical coherence tomography angiography. *Sci Rep*. 2016;6:29064.
67. Sleightholm MA, Arnold J, Kohner EM. Diabetic retinopathy: I. The measurement of intercapillary area in normal retinal angiograms. *J Diabet Complications*. 1988;2:113–116.
68. Chui TY, VanNasdale DA, Elsner AE, Burns SA. The association between the foveal avascular zone and retinal thickness. *Invest Ophthalmol Vis Sci*. 2014;55:6870–6877.
69. Yu PK, Balaratnasingam C, Cringle SJ, McAllister IL, Provis J, Yu DY. Microstructure and network organization of the microvasculature in the human macula. *Invest Ophthalmol Vis Sci*. 2010;51:6735–6743.
70. Sherman TF. On connecting large vessels to small. The meaning of Murray's law. *J Gen Physiol*. 1981;78:431–453.
71. Iwasaki M, Inomata H. Relation between superficial capillaries and foveal structures in the human retina. *Invest Ophthalmol Vis Sci*. 1986; 27:1698–1705.
72. Remky A, Wolf S, Knabben H, Arend O, Reim M. Perifoveal capillary network in patients with acute central retinal vein occlusion. *Ophthalmology*. 1997;104:33–37.
73. Wolf S, Arend O, Schulte K, Ittel TH, Reim M. Quantification of retinal capillary density and flow velocity in patients with essential hypertension. *Hypertension*. 1994;23:464–467.
74. Rutkowski P, May CA. Nutrition and vascular supply of retinal ganglion cells during human development. *Front Neurol*. 2016;7:49.
75. Michaelson IC. *Retinal circulation in man and animals*. Springfield, IL: Charles C. Thomas; 1954:74–100.
76. Bek T, Jensen PK. Three-dimensional structure of human retinal vessels studied by vascular casting. *Acta Ophthalmol (Copenh)*. 1993;71:506–513.
77. Snodderly DM, Weinhaus RS, Choi JC. Neural-vascular relationships in central retina of macaque monkeys (Macaca fascicularis). *J Neurosci*. 1992;12:1169–1193.
78. Chui TY, Gast TJ, Burns SA. Imaging of vascular wall fine structure in the human retina using adaptive optics scanning laser ophthalmoscopy. *Invest Ophthalmol Vis Sci*. 2013;54:7115–7124.
79. Phelps DL. Oxygen and developmental retinal capillary remodeling in the kitten. *Invest Ophthalmol Vis Sci*. 1990;31:2194–2200.
80. Jia Y, Bailey ST, Hwang TS, et al. Quantitative optical coherence tomography angiography of vascular abnormalities in the living human eye. *Proc Natl Acad Sci U S A*. 2015;112:E2395–2402.
81. Simundic AM. Measures of Diagnostic Accuracy: Basic Definitions. *EJIFCC*. 2009;19:203–211.
82. Chui TY, Pinhas A, Gan A, et al. Longitudinal imaging of microvascular remodelling in proliferative diabetic retinopathy using adaptive optics scanning light ophthalmoscopy. *Ophthalmic Physiol Opt*. 2016;36:290–302.
83. Campochiaro PA, Wykoff CC, Shapiro H, Rubio RG, Ehrlich JS. Neutralization of vascular endothelial growth factor slows progression of retinal nonperfusion in patients with diabetic macular edema. *Ophthalmology*. 2014;121:1783–1789.
84. Fu X, Gens JS, Glazier JA, Burns SA, Gast TJ. Progression of diabetic capillary occlusion: a model. *PLoS Comput Biol*. 2016;12:e1004932.
85. Pinhas A, Razeen M, Dubow M, et al. Assessment of perfused foveal microvascular density and identification of nonperfused capillaries in healthy and vasculopathic eyes. *Invest Ophthalmol Vis Sci*. 2014;55:8056–8066.
86. Sakata K, Funatsu H, Harino S, Noma H, Hori S. Relationship between macular microcircula-

tion and progression of diabetic macular edema. *Ophthalmology*. 2006;113:1385–1391.

87. Funatsu H, Sakata K, Harino S, Okuzawa Y, Noma H, Hori S. Tracing method in the assessment of retinal capillary blood flow velocity by fluorescein angiography with scanning laser ophthalmoscope. *Jpn J Ophthalmol*. 2006;50:25–32.
88. Wolf S, Arend O, Toonen H, Bertram B, Jung F, Reim M. Retinal capillary blood flow measurement with a scanning laser ophthalmoscope. Preliminary results. *Ophthalmology*. 1991;98:996–1000.
89. Tokayer J, Jia Y, Dhalla AH, Huang D. Blood flow velocity quantification using split-spectrum amplitude-decorrelation angiography with optical coherence tomography. *Biomed Opt Express*. 2013;4:1909–1924.